Int. J. Multiphase Flow Vol. 6, pp. 173–190
Pergamon/Elsevier, 1980. Printed in Great Britain

A CO-CURRENT STRATIFIED AIR–MERCURY FLOW WITH WAVY INTERFACE

M. AKAI, A. INOUE, S. AOKI and K. ENDO
Research Laboratory for Nuclear Reactors, Tokyo Institute of Technology, Meguro-ku, Tokyo, Japan

(*Received* 8 *August* 1979; *in revised form* 25 *October* 1979)

Abstract—Horizontal, co-current, stratified, air-mercury flow in a rectangular channel has been studied experimentally and analytically as a basic study for magnetohydrodynamic two-phase flow.

The flow regime is identified by examining the structure of interfacial waves. The pressure drop and the holdup data are presented in terms of conventional Lockhart–Martinelli parameters. From the measurement of gas phase velocity profile, it is shown that, for wavy interface regime, the plane of maximum velocity shifts progressively towards the smooth upper wall as the gas flow rate is increased, and the interfacial region exhibits the similar characteristics as the turbulent flow over a rough surface.

An analytical method for the stratified flow, considering the wave-induced shear stress of the form

$$-\rho\overline{\tilde{u}\tilde{v}}/\tau_i = A\exp(-Cy^+),$$

is developed. The necessary constants are fitted to available data, and the numerical results for the air-mercury flow are obtained. These results show reasonable agreement with the experimental data.

1. INTRODUCTION

A liquid metal–helium two-phase flow has been considered to be one of the adequate methods for a cooling system in a fusion reactor. One proposed method is to employ a stratified or an annular-dispersed flow, because it is possible that thermo-hydraulic requirements, i.e. reducing the MHD pressure loss and attaining the high heat transfer rate, are well satisfied. In these flow regimes, however, there exist uncertain problems which are not only transport mechanisms in the vicinity of wavy gas–liquid interface but also effects of electro-magnetic fields on a conductive liquid film flow.

These flow regimes may be perhaps the simplest ones to investigate among various types of two-phase flow, because the theoretical analysis as well as the experimental techniques are considered to be the applications of those for a single-phase flow. Even when excluding the problem of electro-magnetic effects on liquid film, however, there are still many difficulties in modelling the effects of disturbed interfacial waves for the problem of heat, mass or momentum transfer across the interface. For example, in annular-dispersed flow, though it is expected that the characteristics of the gas–liquid interface greatly affect these transport processes, there seem few satisfactory results for this problem through lack of sufficient information concerning the turbulent structure of both phases in the vicinity of the sheared and disturbed interface.

Horizontal, stratified, two-phase flow which represents some of the typical features of the annular two-phase flow has been widely studied experimentally and analytically to elucidate various characteristics of the two-phase flow.

Hanratty & Engen (1957) classified the flow regimes observed for a fixed liquid flow rate as the gas flow rate is increased. They are: (a) smooth surface, (b) two-dimensional waves, (c) three-dimensional waves, (d) roll waves and (e) atomization. Ellis & Gay (1959) also investigated these flow regimes to determine the interfacial shear stress and roughness characteristics of the water surface through the air velocity profile measurement. In our previous paper (Akai *et al.* 1977), the stratified air–water flow in a horizontal rectangular channel was studied experimentally giving attentions mainly to the velocity fluctuations in both phases exerted by the interfacial waves, and it was confirmed that the eddy viscosities in the vicinity of the wavy interface present much larger values than that obtained for the region close to a smooth wall in the single-phase turbulent flow.

The work by Lockhart & Martinelli (1949) is one of the earliest studies to predict analytically the pressure drop and the holdup for two-phase gas–liquid flow. Though this attempt may be the simplest one and applicable to all flow regimes, relatively low accuracy is attained due to its flexibility. For example, as suggested by many researchers, the measured pressure drops for stratified or wavy two-phase flow are always smaller than those predicted according to the Lockhart–Martinelli method. Moreover the calculated values of holdup are also in error sometimes up to more than 100 per cent, compared to the experimental values. These large deviations are inconsistent with the fact that the stratified two-phase flow is the flow pattern most closely approximated by the Lockhart–Martinelli model.

From this point of view, there have been a number of analytical studies to predict the pressure drop and the holdup or to improve the Lockhart–Martinelli correlation. Among these active studies, Johannessen (1972) analyzed a stratified turbulent–turbulent flow in a circular tube, introducing some simplifications to neglect the interfacial shear stress. Johannessen's work is perhaps the first one to prove theoretically that non-dimensional pressure drop, ϕ_L or ϕ_G, and holdup, $1-\alpha$, are unique functions of variable X, as postulated by Lockhart and Martinelli. Recently Aggour & Sims (1978) proposed a theoretical model for the stratified two-phase flow between parallel plates, taking into account the interfacial shear stress and considering the smooth moving interface. And with some simplifications, they proposed algebraic equations which gave relations between Lockhart–Martinelli parameters, providing fairly good predictions for the pressure drop and the holdup in both rectangular channel and circular tube. In none of above mentioned work. however, does one find direct solutions of momentum equations for both phases, or a little consideration as to the effects of interfacial waves.

In the present paper, we first describe the results of experimental work for co-current, stratified, air-mercury flow in a rectangular channel. The purpose of this experiment is to obtain background data for the magnetohydrodynamic two-phase flow which, as explained in the opening sentences, is considered to be applicable to the cooling system for the controlled fusion reactor. The experimental study about the MHD two-phase flow is now being conducted at our laboratory and the results will be reported on another occasion. The second half of the present paper deals with the analysis of stratified two-phase flow between two parallel plates, taking into account a wave-induced turbulence, and provide direct solutions of momentum equations for the turbulent–turbulent case. And we give this problem our general considerations based on the results of numerical analysis and experiment.

2. EXPERIMENTAL APPARATUS

A diagram of the apparatus set up for the air–mercury stratified two-phase flow experiment is given in figure 1. The experiment was conducted in a rectangular test channel fabricated with 6 mm thick acrylic resin. The internal dimensions of this channel were 48 mm wide and 18 mm high, with the total length 3.6 m. This rectangular channel was precisely held horizontal using leveling technique.

The measuring portion was located at a distance of about 3 m from the inlet of the test channel. This measuring portion was provided with an acrylic block having a guide hole and a fitting which allowed the smooth insertion of a hot-wire probe or a needle probe and gave a sufficient seal. For the measurement of pressure drop, four static pressure taps with 0.5 mm-dia. were mounted at points 50 cm and 25 cm up- and downstream of the measuring portion. These positions of the static pressure taps and the measuring portion were chosen because they gave sufficient length for the flow field, i.e. velocity profile, liquid film thickness and pressure drop to reach their fully developed shape. Preliminary experiments had been conducted to check and confirm this fact.

The test channel was connected to an entrance section in which the flows of supplied air and mercury came in smooth contact and then flowed co-currently into the test channel. After passage through the channel, the flow was led to an air–mercury separator section where the

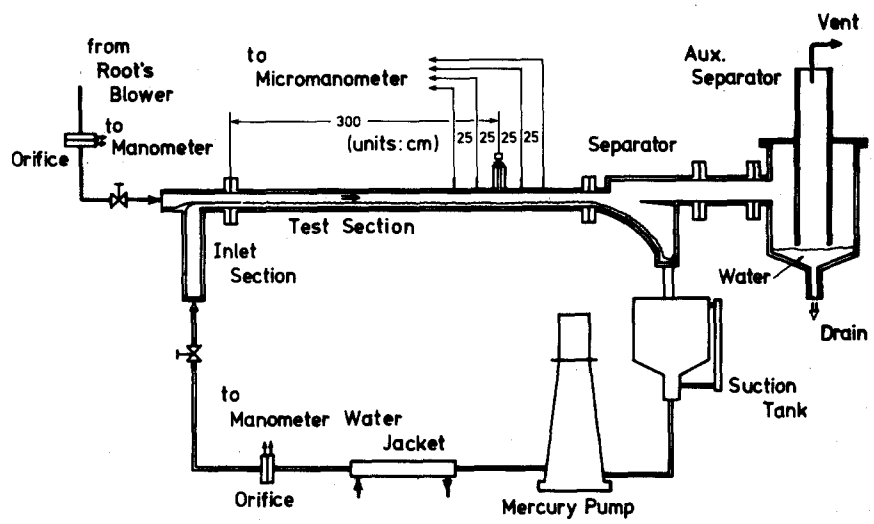

Figure 1. Diagram of experimental apparatus.

mercury was separated from the air and flowed down to a suction tank. Under some flow conditions, however, there was a danger of the separated air still containing fine mercury droplets. Therefore the air from the separator was further led to an auxiliary separator in which the air collided with water surface and the remained mercury was finally eliminated from the air. The monitoring of the released air has been conducted and no indication of existance of mercury vapor has been suggested.

The inlet section and the suction tank were connected with a stainless steel closed loop through which the mercury was circulated continuously by a centrifugal mercury-pump. The flow rate of the mercury was regulated by a glove valve, and measured by orifice. Mercury temperature control was facilitated by means of water jackets located before the inlet section. The air was supplied from a Root's blower equipped with a filter and an after-cooler. Flow control was done by a pressure regulating valve and a glove valve. The flow rate of the air was determined also by measuring orifice.

In this manner the flow rates of the air and the mercury were adequately controlled and the temperature of the flow field was kept constant within ± 0.5°C over a set of runs.

3. INSTRUMENTATION

In the present experiment, pressure drop, liquid film thickness, wave pattern and velocity profile in the gas phase were measured in the stratified two-phase flow. A differential pressure micromanometer was used for pressure drop measurement. It was possible to read the differential pressure to ± 0.01 mmAq in the range 0–20 mmAq. Other details of the measurement are shown below.

3.1 *Measurement of air velocity*

All velocity data were obtained by a linearized constant-temperature hot-wire anemometry system. For the measurement of air velocity apart from the air–mercury interface, tungsten hot-wire probes, with diameter of 5 μm and 1 mm of active sensor length, were provided. These probes, however, could be subjected to destructive damage by hitting of mercury surface waves. Therefore, it was impracticable to obtain the velocity information close to the interface. For this reason, quartz-coated hot-film probes (Thermo-Systems Inc., Model 1210-60W) were used, with overheating about 15°C, for the measurement of air velocity close to the air–mercury interface. All of these probes were single wired sensors, and positioned in the measuring portion with each axis parallel to the bottom wall of the channel and perpendicular to the flow direction. Consequently the mean and the fluctuating velocities in the direction of the flow

could be measured. These probes were traversed vertically by a micrometer head and the location of them within the channel was determined using a reading microscope and a reference mark on the channel side a known distance from the channel bottom wall. The accuracy of the positioning of the probe was ± 0.02 mm.

The output signals of the anemometer were processed in terms of probability density functions to determine the mean and the fluctuating velocity of the air. Especially when measuring the velocity data very close to the disturbed interface where the air and the mercury appeared alternately, the air signals could be clearly distinguished from the mercury signals because of their significant level difference. This procedure had been conducted in air–water system, and the details can be seen in Akai *et al.* (1977).

3.2 *Measurement of liquid film thickness and wave structures*

A widely applied needle contact method (e.g. Hewitt & Hall-Taylor 1970) was used for the measurement of liquid film thickness, wave amplitude and wave period. The needle probe was made of stainless steel with the diameter of 0.1 mm and was insulated except for the contact point at the tip. In the air–mercury system, the contact is well distinguished due to the high conductivity of the mercury. Therefore the probe was connected to a comparator circuit whose output signals were + 15 V at the contact and 0 V at the no-contact. The needle probe was traversed vertically across the channel by the micrometer head described above, and the square wave output from the comparator was then introduced to a Correlation & Probability Analyzer to obtain the curve of the contact probability vs the distance from the bottom wall and the contact frequency. The liquid film thickness was defined as the distance from the bottom wall to the plane where there is 50 per cent relative contact probability.

4. EXPERIMENTAL RESULTS AND DISCUSSIONS

4.1 *Flow regimes of horizontal air–mercury flow*

In order to characterize the flow regime of the stratified air–mercury flow, the structure of the interface has to be determined. In our previous paper (Akai *et al.* 1977), the interfacial structure of air–water system was identified by comparison between the auto-correlation functions obtained from the signals of the surface displacement probe and the observed wave patterns. The similar method was used to distinguish the wave patterns in the air–mercury system.

The observed flow patterns under the experimental conditions were almost identical to those previously reported for air–water system (Hanratty & Engen 1957, Ellis & Gay 1959, Akai *et al.* 1977). At low mercury flow rate, however, the liquid film began to break at some portions of the test channel as the gas flow rate was increased, and the mercury film exhibited the discontinuity along the flow direction and amoebic films with the length of 3–10 cm travelled by the drag of the gas flow. With further increase in gas flow rate, pebble-like flow pattern sometimes accompanied by atomized mercury was observed. At higher liquid flow rate, on the other hand, the equilibrium interface became unstable and the roll waves continued to grow as the gas flow rate was increased. And finally, the one of these waves plugged the air passage leading to the slug formation. These flow regimes are shown in figure 2.

Figure 2 is a flow map for the horizontal air–mercury flow showing the transitions from smooth surface to two- and three-dimensional waves and to broken film, pebble or slug flow as functions of the gas and liquid Reynolds numbers, Re_G and Re_L, which are based on the depth and the mean velocity of each phase.

In figure 2, the flow regime correlation, calculated with the computer program by Mandhane *et al.* (1974), is superimposed for comparison. It is perhaps not suprising to see the discrepancy between two maps, for the proposed correlation is based mainly on the experimental observations in air–water system.

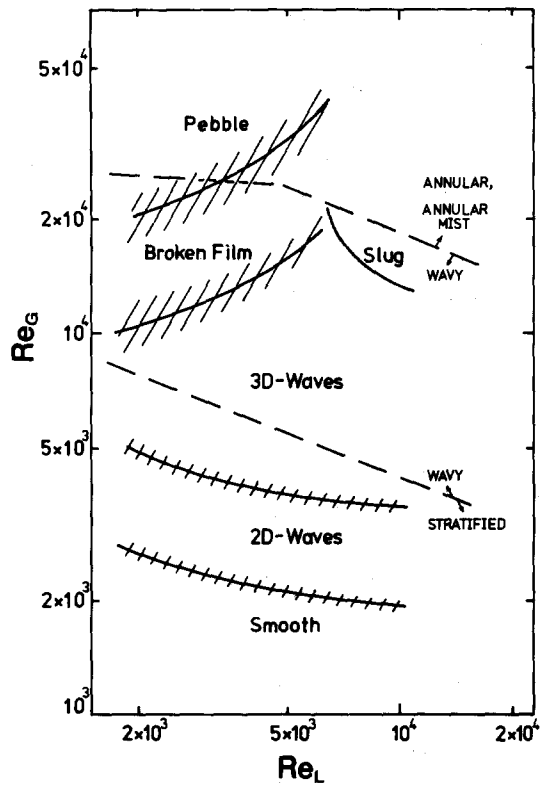

Figure 2. Flow map for horizontal air–mercury flow. ---, proposed line by Mandhane *et al.*

4.2 *Pressure drop and holdup*

All of the pressure drop and the holdup (or the liquid film thickness divided by the channel height) data are presented in terms of the Lockhart–Martinelli parameters in figures 3 and 4. The basic concept of these parameters is that the dimensionless pressure drop ϕ_l and the holdup δ/b are the unique functions of the parameter X, where $X^2 \geq (dP/dx)_L/(dP/dx)_G$ is the ratio of the frictional pressure gradient of the liquid phase to that of the gas phase when each phase flows alone in the channel and $\phi_L^2 = (dP/dx)_{TP}/(dP/dx)_L$ is the ratio of the pressure gradient of the two-phase flow to that of the liquid phase flowing alone in the channel. In these figures, $(dP/dx)_L$ and $(dP/dx)_G$ are estimated using Blasius formula. The solid lines in figures 3 and 4 denote the correlation curves proposed by Aggour & Sims (1978), which are of the form

$$X^2 = 1.189(1-\alpha)^2(2-\alpha)/\alpha^3,$$

$$\phi_L^2 = 0.841/(1-\alpha)^2(2-\alpha),$$

for turbulent–turbulent flow, where α is the void fraction or $1-\delta/b$. These algebraic relations were derived through the analysis of gas–liquid stratified flow between two wide parallel plates taking into account the interfacial shear stress and a smooth, moving interface, together with some simplifications based on the experimental data. And they also concluded that there is essentially a unique relation between the Lockhart–Martinelli parameters ϕ and X and between the holdup and X.

Certainly, it might be possible to say that, when disregarding the liquid flow rate, the experimental results are well correlated in terms of the Lockhart–Martinelli parameters especially in the range $0.1 < X < 1.0$. Here, however, we gave an attention to the dependency to the liquid flow rates and the steeper gradient of the pressure drop to the increment of the gas flow rate than the predicted one, and considered that this discrepancy was mainly due not only

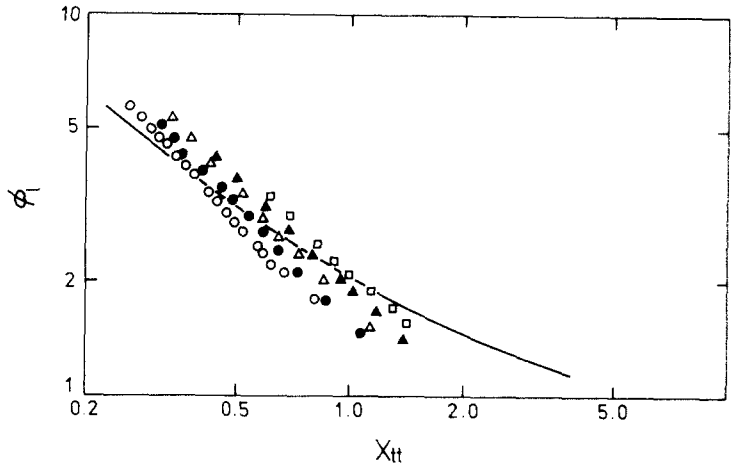

Figure 3. Pressure drop data. ○, $Re_L = 2.49 \times 10^3$; ●, $Re_L = 4.00 \times 10^3$; △, $Re_L = 5.66 \times 10^3$; ▲, $Re_L = 8.04 \times 10^3$; □, $Re_L = 9.87 \times 10^3$. ——, prediction by Aggour and Sims.

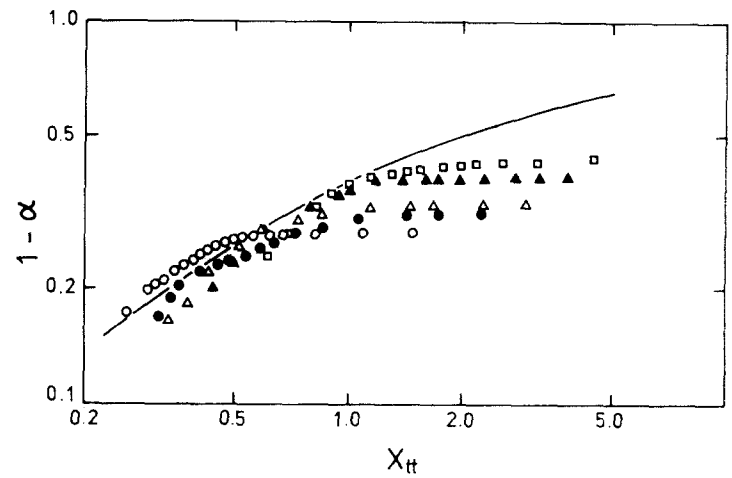

Figure 4. Holdup data (see figure 3 for notation).

to the simplifications employed by Aggour and Sims but also to neglecting the effect of the interfacial waves.

4.3 *Gas phase velocity profiles and friction factors*

Figure 5 shows the gas mean velocity profiles for three representative runs, in which the liquid flow rate is kept constant. In figure 5, the distance from the interface and the mean velocity are normalized by the gas phase thickness and the maximum velocity respectively, and $(Re_G)_{eq}$ denotes the gas Reynolds number based on the mean velocity and the equivalent diameter of the gas phase. When the flow is in smooth interface region, the plane of maximum velocity ($y = y_p$) is located slightly below the central plane of the gas phase. For the wavy interface regime, on the other hand, the plane of maximum velocity shifts progressively towards the smooth upper wall as the gas phase Reynolds number is increased, showing that the interfacial shear stress (τ_i) becomes more than three times as much as that at the upper wall (τ_L). This shift of the maximum and associated velocity profile distorition have been also reported by many workers (Theofanous *et al.* 1976; Akai *et al.* 1977) for air–water system, and is considered to cause the increase in the pressure drop. The similar phenomenon has been observed by Hajalić & Launder (1972) in an asymmetric single-phase flow in a plane channel, in which a roughened wall influences the flow as the wavy interface does in the present study.

A few typical examples of dimensionless velocity profiles are illustrated in the usual

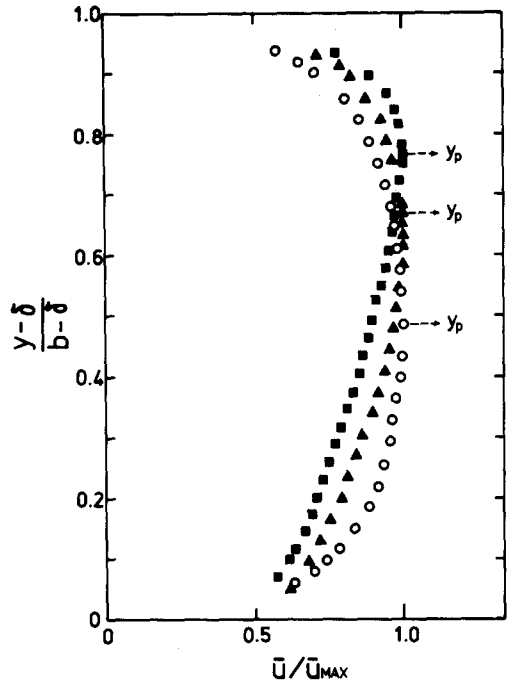

Figure 5. Mean velocity profiles for gas phase. $Re_L = 8.04 \times 10^3$. ○, $(Re_G)_{eq} = 3.69 \times 10^3$ (smooth interface); ▲, $(Re_G)_{eq} = 1.05 \times 10^4$; ■, $(Re_G)_{eq} = 2.07 \times 10^4$.

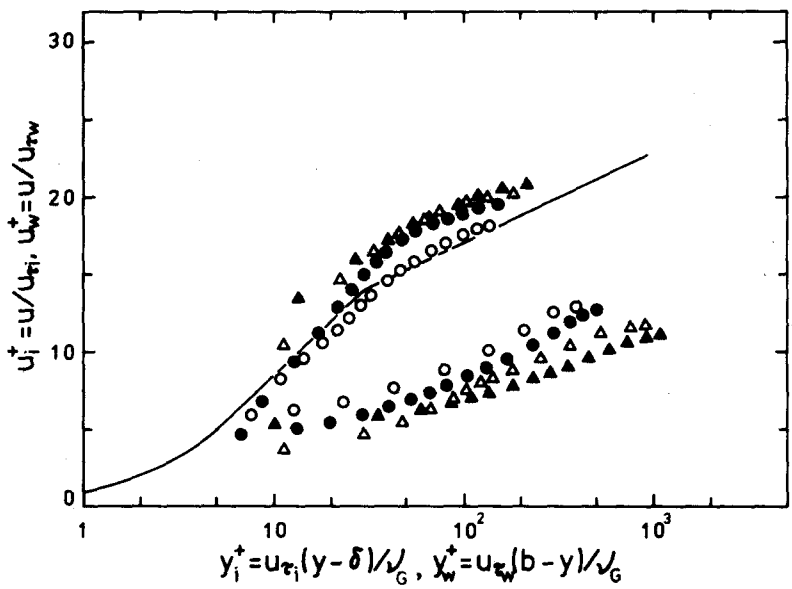

Figure 6. Semi-log plot of mean velocity profiles for gas phase. $Re_L = 8.04 \times 10^3$. ○, $(Re_G)_{eq} = 1.05 \times 10^4$; ●, $(Re_G)_{eq} = 1.36 \times 10^4$; ł, $(Re_G)_{eq} = 2.07 \times 10^4$; ▲, $(Re_G)_{eq} = 2.76 \times 10^4$. ——, universal velocity profile.

semi-log fashion in figure 6. In the figure, $u_i^+ - y_i^+$ refers to the velocity profiles in the region between the interface and y_p, and $u_w^+ - y_w^+$ to the upper wall region which are normalized by the interfacial friction velocity or the upper wall friction velocity respectively. The shear stresses were determined with the knowledge of y_p and the pressure drop utilizing the method of Hanratty & Engen (1957). The well known universal velocity profile is shown for comparison. In the interfacial region, a downward, nearly parallel shift from the universal velocity profile is observed with increasing gas phase Reynolds number. This trend corresponds to the remarkable increase in the interfacial shear stress mentioned above, and is a well known characteristic of the rough wall turbulence.

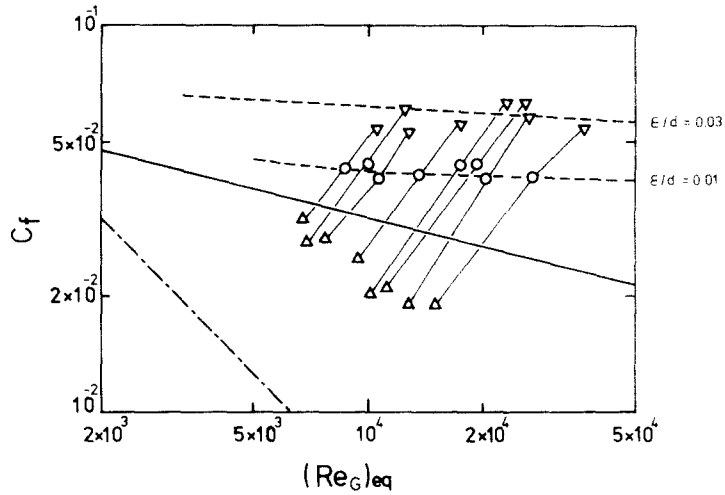

Figure 7. Friction coefficient for gas phase. $Re_L = 8.04 \times 10^3$. ▽, interface region; △, upper wall region; ○, bulk. ———, single-phase turbulent line; —·—, laminar line; – – –, rough wall correlations.

In the upper wall region, on the contrary, the velocity profile data lie closer to the universal profile and have a tendency to shift slightly upward for $y_w^+ > 20$ with increasing Reynolds number, and moreover, the tendency is similar to that observed for low Reynolds number turbulence (Patel & Head 1969). This phenomena may be considered as follows: the significant increase of y_p or the decrease of τ_L compared with τ_i causes the equivalent diameter of the upper wall region to be small, leading to decrease of "superficial" Reynolds number of this region so that the velocity profile shows the trend as described above.

From above results, it is suitable to consider the gas phase friction factor in a separate manner (upper wall and interfacial region). Figure 7 shows the friction factors for the upper wall and the interfacial region and for the total gas phase as functions of equivalent Reynolds number. The commonly accepted formulae and the correlation for the rough pipe flow including the roughness parameters are also superimposed. The solid lines connecting the datum points indicate that they are obtained from a run. It is clear from figure 7 that when gas flows above wavy interface, the interfacial friction factors exhibit a behavior similar to that for the rough wall, while in the upper wall region the friction factors give lower values than estimated for the smooth wall turbulence.

4.4 *Eddy viscosity profiles*

The eddy viscosity profiles in the gas phase were estimated from the results of the pressure drop and the velocity profile measurement. The calculated eddy viscosity profiles for the set of runs presented above are shown plotted in figures 8 and 9. The solid lines denote the profiles for single-phase, smooth wall turbulence evaluated by [6], described later. In these figures, the plotted values are to be considered as the total of the eddy viscosities representing the sum of the eddy viscosity for the background turbulence and that for the wave-induced turbulence. The analysis to be presented is based on this concept.

The eddy viscosity profiles in the upper wall region (figure 8) are in agreement with those predicted for ordinary turbulent fields, except for the central region of the gas phase where the velocity gradient is so small that the obtained values for this region might contain rather a fairly larger amount of errors than those for near the wall. Consequently it seems to suggest that the turbulent structure near the upper wall is similar to that of single-phase turbulence along a smooth flat plate, i.e. there may be little effect of the wavy moving boundary at the opposite side.

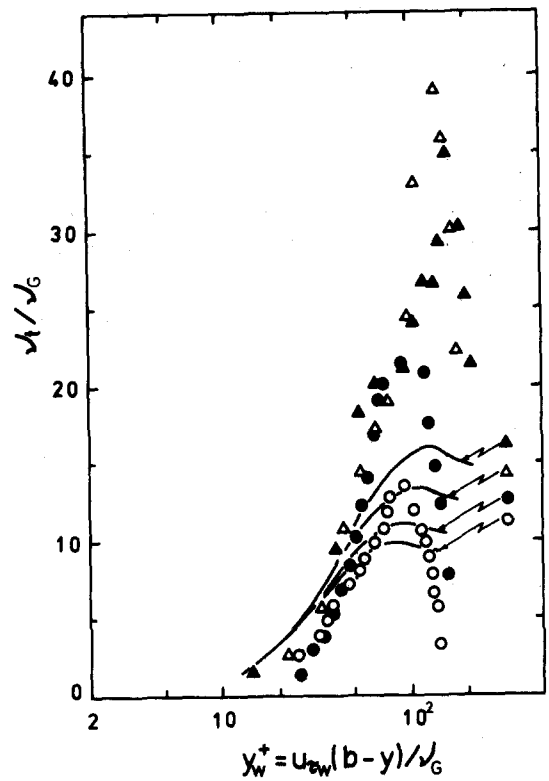

Figure 8. Eddy viscosity profiles for upper wall region. ○, $(Re_G)_{eq} = 1.05 \times 10^4$; ●, $(Re_G)_{eq} = 1.36 \times 10^4$; △, $(Re_G)_{eq} = 2.07 \times 10^4$; ▲, $(Re_G)_{eq} = 2.76 \times 10^4$. ——, estimation by [6].

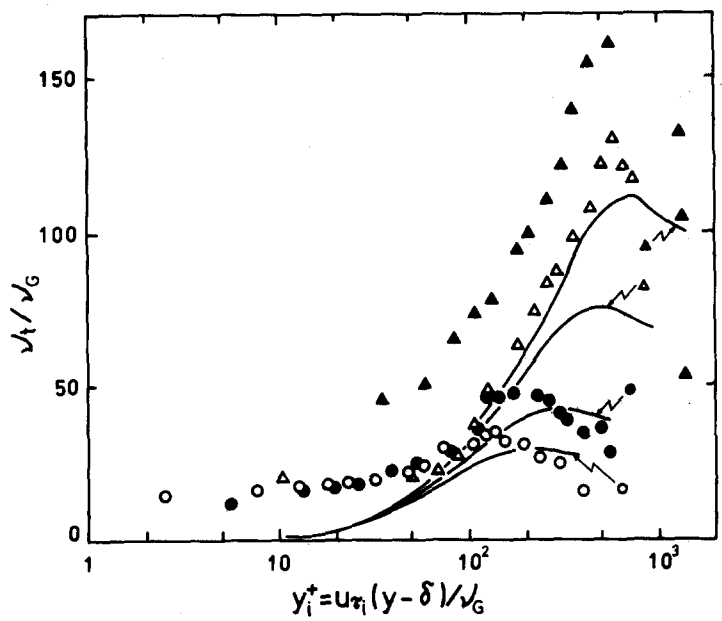

Figure 9. Eddy viscosity profiles for interface region (see figure 8 for notation).

As expected from the results of the velocity profile, the eddy viscosity profiles obtained in the interfacial region (figure 9) exhibit much larger values, especially in the vicinity of the interface, than those predicted for a single-phase flow. It is considered that the excess eddy viscosity near the disturbed interface indicates the sensitive effect of the wavy boundary. The similar results about the behavior of the eddy viscosity near the wavy interface were also

reported for air–water system by Alkai *et al.* (1977). It is clearly evident from the results that a large amount of momentum transfer should occur in the vicinity of the wavy interface.

5. ANALYSIS

The proposed model assumes that the two-phase stratified flow in a rectangular channel is adequately represented by the two-dimensional flow between two parallel plates. The aspect ratio of the rectangular channel used in the experiment may not be large enough for the flow to be assumed two-dimensional. It was confirmed, however, from the experiments of turbulent air flow in this channel, that the skin friction coefficient or the velocity profile data agreed to the well known results by Patel & Head (1969) (aspect ratio of 48) within a few per cent of discrepancy. Moreover when considering the stratified flow, the aspect ratio corresponding to each fluid layer becomes larger than that in the case of the single-phase flow. Accordingly, we consider the assumption of two-dimensional flow to be appropriate for the present analysis.

5.1 *Governing equations*

The notation and the coordinate system for the analysis are shown in figure 10. The following fundamental assumptions are made:

(1) Both fluids are incompressible with constant physical properties.

(2) The flow is steady and fully developed turbulence.

The basic concept of the present analysis is that the turbulent field in the stratified flow with wavy interface may be described by superposition of the wave-induced velocity fluctuation on the background turbulence. In order to take into account the wave-induced turbulence, the instantaneous velocity is written as

$$u_i = \bar{u}_i + u_i' + \tilde{u}_i \qquad (i = 1, 2, 3), \tag{1}$$

where $\bar{u}_i$ is the time-averaged mean velocity, u_i' is the background turbulent velocity fluctuation and $\tilde{u}_i$ represents the wave-induced perturbation. It is assumed that u_i' and $\tilde{u}_i$ are statistically independent and the time averaged quantities of these fluctuations are zero.

Substituting [1] into the x-component momentum equation and taking the mean value of it, the equation for the mean velocity is put into the form,

$$\bar{u}\frac{\partial \bar{u}}{\partial x} + \bar{v}\frac{\partial \bar{u}}{\partial y} = -\frac{\partial \overline{u'v'}}{\partial y} - \frac{\partial \overline{\tilde{u}\tilde{v}}}{\partial y} - \frac{1}{\rho}\frac{\partial P}{\partial x} + \nu\frac{\partial^2 \bar{u}}{\partial y^2}, \tag{2}$$

showing the contribution by the additional stress, $-\rho\overline{\tilde{u}\tilde{v}}$, arising from the wave-induced pertubation. Here the continuity equation has been considered. From the assumptions, the

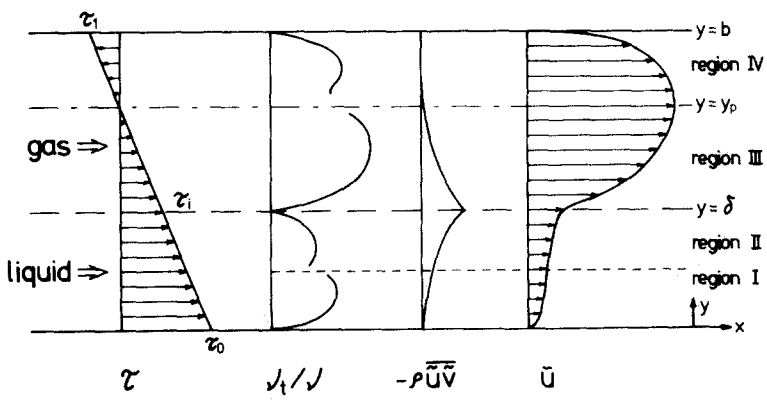

Figure 10. Analytical model.

l.h.s. of [2] can be omitted. Then the mean velocity equation can be integrated to give

$$\tau = \mu \frac{\partial \bar{u}}{\partial y} - \rho \overline{u'v'} - \rho \bar{\tilde{u}}\bar{\tilde{v}}\,, \qquad [3]$$

where τ is the shear stress and is given by

$$\tau = -\frac{\partial P}{\partial x}(y - y_p)$$
$$= \tau_0 - (\tau_0 - \tau_1)\frac{y}{b}. \qquad [4]$$

As mentioned above, the Reynolds stress term, $-\rho\overline{u'v'}$, is treated in terms of the eddy viscosity ν_T. Consequently the mean momentum equation of the form

$$\tau = \mu\left(1 + \frac{\nu_T}{\nu}\right)\frac{d\bar{u}}{dy} - \rho\bar{\tilde{u}}\bar{\tilde{v}}\,, \qquad [5]$$

is applied to each phase.

As to the eddy viscosity, we choose the following expression (McEligot *et al.* 1970)

$$\frac{\nu_T}{\nu} = \frac{\kappa}{6}\left[y^+ - y_L{}^+ \tanh\frac{y^+}{y_L{}^+}\right]\left[2 - \frac{y}{H}\right]\left[1 + 2\left(1 - \frac{y}{H}\right)^2\right], \quad \kappa = 0.4225, \quad y_L{}^+ = 11.0\,, \qquad [6]$$

among a number of empirical formulae by two reasons. First, it describes the velocity distribution of turbulent flow in a duct conveniently from the wall region to the center of the flow, and secondly, it satisfies the computational requirement that the eddy viscosity can be evaluated by the wall shear stress and the distance from the wall.

Because of using [6] in the analysis, the flow field is divided into four regions (figure 10). Application of [5] together with [6] to the region II and III means that, except the wave contribution, the gas–liquid interface is assumed to play a role like a moving wall having the infinitesimal thickness for the behavior of turbulent structure, i.e. the eddy viscosity profiles. Therefore the nondimensional distance y^+ is expressed in four ways according to the shear stresses at the respective boundaries. Furthermore, there is a parameter H in [6] which represents the dimensional effect of flow channel. In the case of single-phase flow, H is chosen as a half depth of the channel, but in the present analysis, the following definition is used:

$$H = \begin{cases} \delta/2 & \text{(region I and II)}, \\ y_p - \delta & \text{(region III)}, \\ b - y_p & \text{(region IV)}. \end{cases} \qquad [7]$$

From above expressions, the resulted eddy viscosity profiles have discontinuities at $y = \delta/2$, y_p, but the results of sensitivity analysis have shown that the calculated pressure drop, liquid film thickness or velocity profile are little affected by the behavior of eddy viscosity at the central region of the flow.

The boundary conditions are as follows:

$$\bar{u}_L = 0 \quad \text{at} \quad y = 0\,,$$
$$\bar{u}_L = \bar{u}_G \quad \text{at} \quad y = \delta\,,$$
$$\bar{u}_G = 0 \quad \text{at} \quad y = b\,,$$

and the continuity of the velocity at $y = \delta/2$ and $y = y_p$ is to be considered.

5.2 *Estimation of wave-induced turbulence*

To complete the simulation of [3], attention is now given to the wave-induced shear stress term, $-\rho\tilde{u}\tilde{v}$. There may be some possible expression for this term, e.g. to describe the term by equivalent eddy viscosity similar to the background turbulence, or to use the mixing length hypothesis considering that the behavior of the wave-induced turbulence is mainly dominated by the length scale parameters such as wave amplitude or wave length. To determine which expression be most adequate to the present analysis, the total eddy viscosity obtained in the experiment (figure 9) was examined and it was confirmed that rather a direct simulation of the wave-induced stress might be more convenient than the methods mentioned above. Figure 11 shows the calculated wave-induced shear stress in the gas phase normalized by the interfacial shear stress τ_i, as a function of nondimensional distance from the interface. The value of the wave-induced shear stress was estimated assuming that the total eddy viscosity is the sum of the eddy viscosity of the background turbulence expressed by [6] and that of the wave-induced one. Hence the wave-induced shear stress was calculated from the excess eddy viscosity and the velocity profile according to [5].

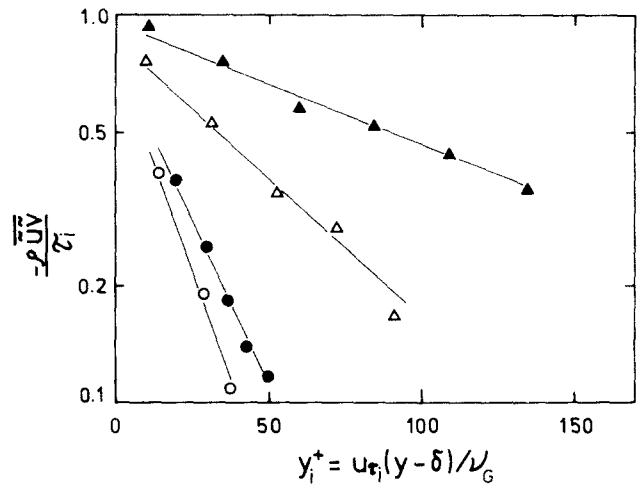

Figure 11. Wave induced shear stress. $Re_L = 8.04 \times 10^3$. ○, $(Re_G)_{eq} = 1.05 \times 10^4$; ●, $(Re_G)_{eq} = 1.36 \times 10^4$; △, $(Re_G)_{eq} = 2.07 \times 10^4$; ▲, $(Re_G)_{eq} = 2.76 \times 10^4$.

The estimated values for $-\rho\tilde{u}\tilde{v}/\tau_i$ have, of course, some errors arising from the differentiating procedure, but figure 11 indicates that the wave-induced shear stress may be expressed as

$$-\frac{\rho\tilde{u}\tilde{v}}{\tau_i} = A\exp(-Cy^+), \qquad [8]$$

where the parameter A denotes the rate of the wave-induced shear stress to the total shear stress at the interface, and C is a damping factor which is written as C_G for the gas phase and C_L for the liquid phase.

This exponential feature of the damping of the wave-induced shear stress is similar to that of the flow generated by an oscillating flat plate, and considered to be reasonable for the present case. The wave-induced shear stress in the liquid phase cannot be estimated because of the absence of the velocity data. But in our previous study on air–water system, the velocity profile and the velocity fluctuation in wavy water film flow were measured and excessive eddy viscosity was also distinguished. With this fact and a physical consideration it is satisfactory to consider that the same idea might be applied to the mercury flow. Consequently, the wave-induced shear stress in both phases are written in the form:

For liquid phase:

$$-\frac{\rho_L\overline{\tilde{u}_L\tilde{v}_L}}{\tau_i} = A\exp\left(-C_L\frac{\delta-y}{\nu_L}\sqrt{\left(\left|\frac{\tau_i}{\rho_L}\right|\right)}\right). \quad [9]$$

For gas phase:

$$-\frac{\rho_G\overline{\tilde{u}_G\tilde{v}_G}}{\tau_i} = A\exp\left(-C_G\frac{y-\delta}{\nu_G}\sqrt{\left(\left|\frac{\tau_i}{\rho_G}\right|\right)}\right). \quad [10]$$

The values of A, C_L and C_G will be considered later.

5.3 *Numerical treatment*

Flow characteristics of the stratified two-phase flow should be analyzed if the flow rates of both fluids and the dimensions of the channel were given. In the present analysis, however, there exist unknown variables such as δ, τ or y_p which not only are necessary to describe the eddy viscosity and the wave-induced shear stress but also affect each other in a sensitive and complicated manner. Therefore it is difficult to solve the equations with the given values of Q_L (volumetric liquid flow rate per unit width) and Q_G (volumetric gas flow rate per unit width). Accordingly the shear stress at the lower wall τ_0 and the flow rate of the liquid Q_L are chosen as an input condition, and the following numerical procedure is taken:

(1) Assume the shear stress at the upper wall (τ_L).

(2) Assume the liquid film thickness (δ), and calculate the eddy viscosity profiles for the four regions and the wave-induced shear stress in each phase.

(3) Integrate the momentum equation for liquid phase to obtain the velocity profile ($\bar{u}_L$).

(4) Calculate the liquid flow rate (Q_{Lc}) from the obtained velocity profile.

(5) Examine whether $|Q_L - Q_{Lc}|$ is less than the permissible error, and if not, correct δ and repeat the process from (2).

(6) If $Q_{Lc} = Q_L$, calculate the gas phase velocity profile ($\bar{u}_G$) by integrating the momentum equation.

(7) Examine whether $\bar{u}_G(b) = 0$, and if not, correct τ_L and repeat the process from (1).

(8) If the solution which satisfies the boundary conditions and given input condition are obtained, calculate the gas flow rate Q_G and print out the results.

A flow diagram of the computation is shown in figure 12.

6. ANALYTICAL RESULTS AND DISCUSSIONS

The purpose of the present analysis is not only to predict the pressure drop or the holdup of the stratified flow but also to obtain empirical values for A, C_L and C_G which explain the experimental results in a generic manner. For the behavior of the wave-induced shear stress in the gas phase, the useful information can be obtained from figure 11. This figure indicates that the variations in the volumetric flow rate of the gas phase have a significant effect to the damping factor C_G, i.e. C_G decreases as the gas flow rate is increased, while the value of A remains nearly constant. The same tendency might be assumed for the liquid phase. Based on the parameter values estimated from figure 11, and through a large number of numerical experiments, the following expressions

$$A = 0.70, \quad [11]$$

$$C_L = 84.8(1-\tau_i/\tau_0)^{17.8}, \quad [12]$$

$$C_G = 4.8\times10^{-5}(1-\tau_L/\tau_i)^{13.7}, \quad [13]$$

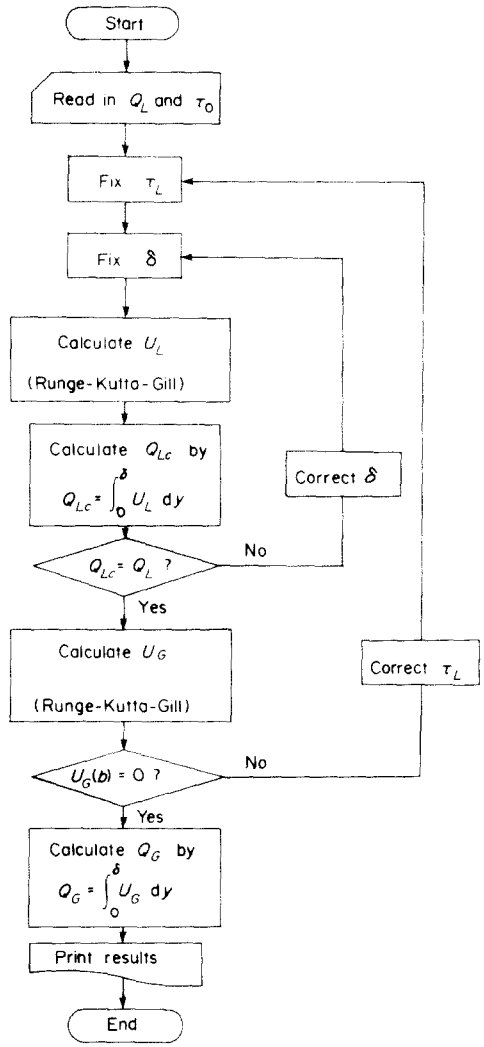

Figure 12. Flow diagram.

were obtained as empirical functions. These expressions were chosen because they gave satisfactory descriptions for the pressure drop or the holdup as well as the distortion of the velocity profile in the gas phase mentioned before over the range of the experimental conditions. For the present case, the order of magnitude for C_L and C_G are 10^{-5} and 10^{-2} respectively. These small values of the damping factors indicate that the disturbances exerted by the interfacial waves extend their influence to the whole flow field.

Further considerations are made as follows: for the liquid phase, the interfacial waves act as turbulent energy source and the produced energy is transported progressively toward the lower wall region; and for the gas phase, though the damping factor is larger than that for the liquid phase, the asymmetric behavior of the total eddy viscosity introduced by the wave-induced shear stress causes a significant distortion of the velocity profile in the gas phase.

Figures 13–15 show typical results for the velocity profiles. The experimental data for the corresponding volumetric flow rates are also shown for comparison in figures 14 and 15. Figure 13 refers to the smooth interface condition, i.e. $-\rho\widetilde{u}\widetilde{v} = 0$, in which the resulted gas flow rate is nearly the same to that of the data shown in figure 14. In this figure, the position of the maximum velocity lies slightly below the center of the gas phase due to the moving interface. The velocity profiles for the wavy interface are shown in figures 14 and 15. For both cases, the distortion of the velocity profile is well reproduced. In all figures, the calculated velocity profiles are in good agreement with the measured ones.

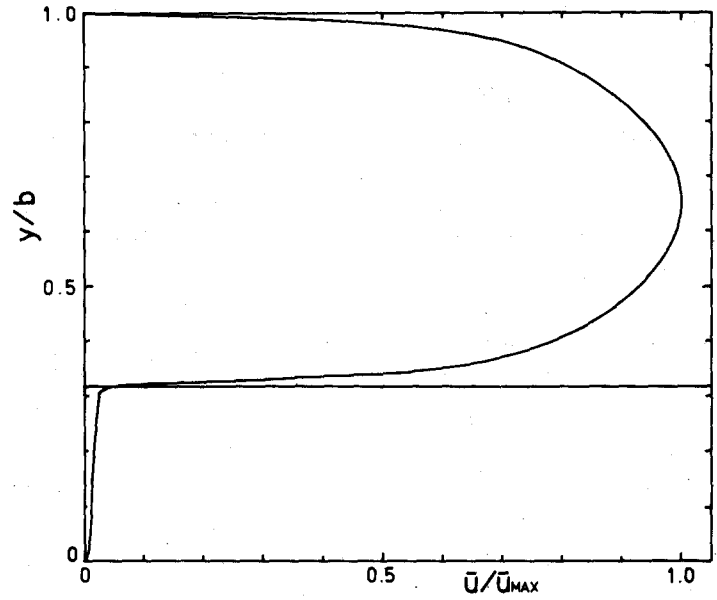

Figure 13. Mean velocity profile prediction with $-\rho\overline{\tilde{u}\tilde{v}} = 0$. $Re_L = 8.04 \times 10^3$, $Re_G = 6.53 \times 10^3$.

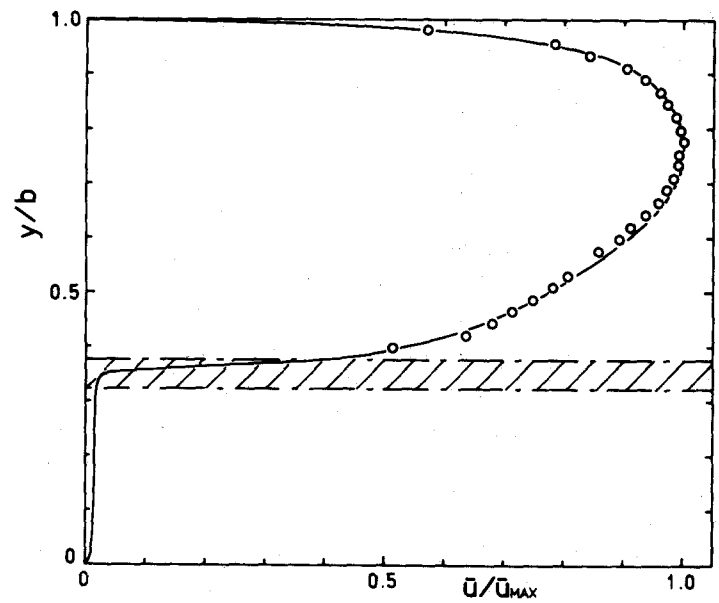

Figure 14. Mean velocity profiles. $Re_L = 8.04 \times 10^3$, $Re_G = 6.51 \times 10^3$. //////, waves. O, experiment; ——, prediction.

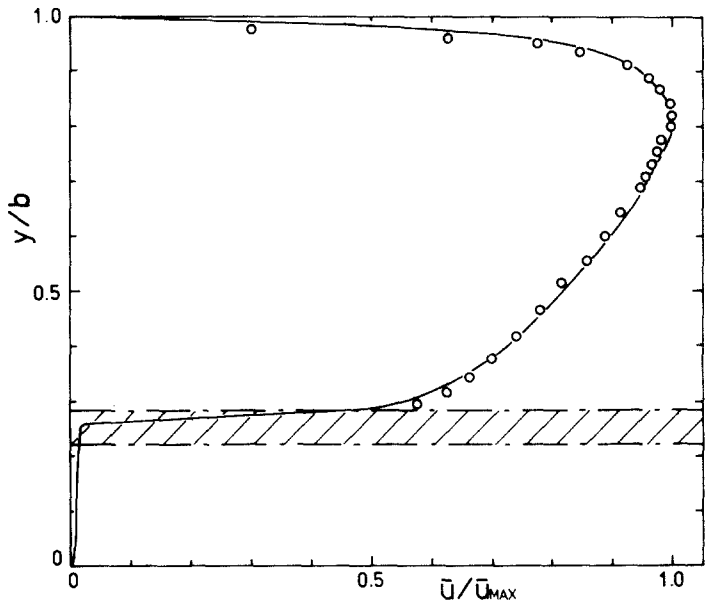

Figure 15. Mean velocity profiles. $Re_L = 8.04 \times 10^3$, $Re_G = 1.24 \times 10^4$. //////, waves. ○, experiment; ——, prediction

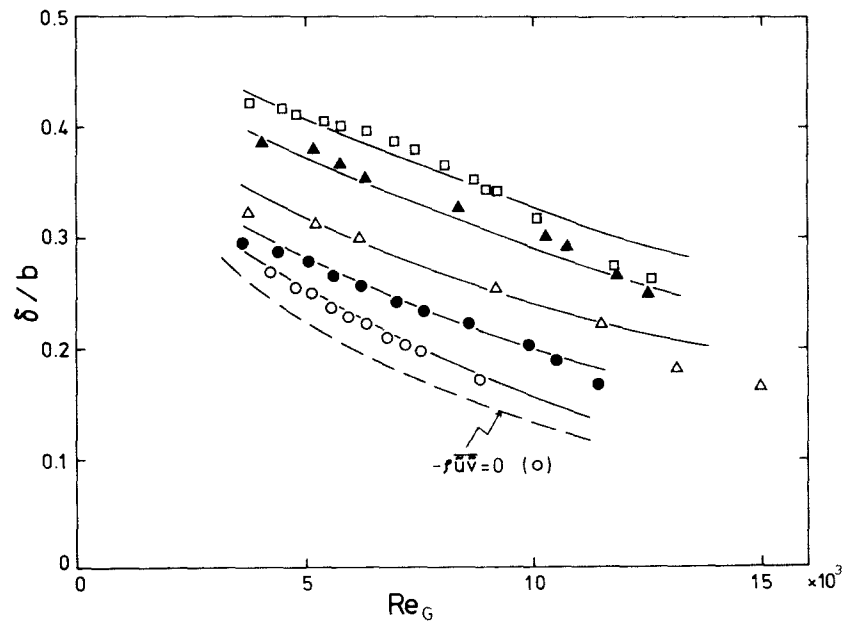

Figure 16. Liquid film thickness. ○, $Re_L = 2.49 \times 10^3$; ●, $Re_L = 4.00 \times 10^3$; △, $Re_L = 5.66 \times 10^3$; ▲, $Re_L = 8.04 \times 10^3$; ○, $Re_L = 9.87 \times 10^3$. ——, prediction.

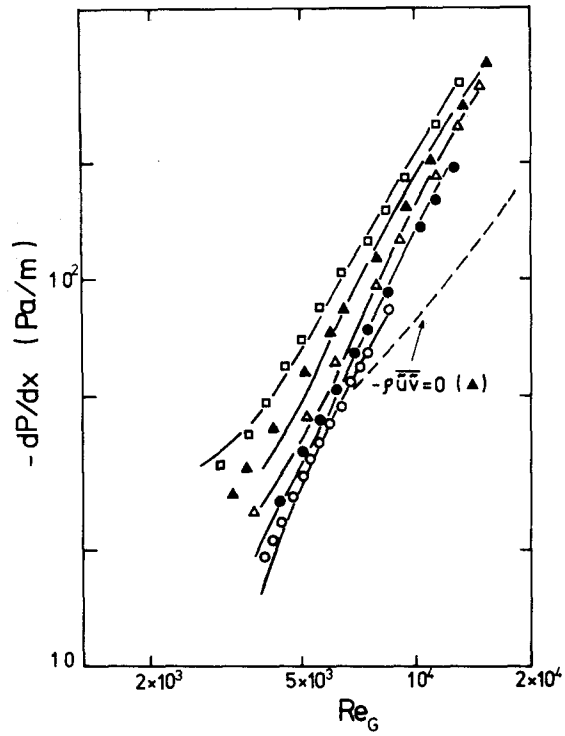

Figure 17. Pressure drop (see figure 16 for notation).

The calculated holdup and pressure drop are compared to experimental results in figures 16 and 17 as a function of gas flow rate. The numerical results for the smooth interface case are also shown for reference. The smooth interface assumption seems to slightly underestimate the holdup as shown in figure 16. While in figure 17, the pressure drop predicted regardless of the wave effect is significantly smaller than the experimental value especially at large Re_G. For both figures, the analytical results taking into account the wave-induced turbulence agree well to the experimental ones.

Considering these analytical results and the experimental results described in the previous section, it is confirmed that the existence of the interfacial waves in a stratified two-phase flow causes an increase in eddy viscosities near the interface which leads to a remarkable distortion of gas phase velocity profile and an increase in pressure drop compared to the smooth interface case. These tendencies are well described by the concept of wave-induced turbulence.

7. CONCLUSIONS

The characteristics of a horizontal stratified air–mercury flow was investigated experimentally and analytically. The results are summarized as follows:

(1) The flow map of horizontal stratified air–mercury flow was presented. Under some flow conditions, the discontinuous mercury film flow was observed.

(2) The pressure drop and the holdup were moderately correlated in terms of the Lockhart–Martinelli parameters. But the dependency on the liquid flow rate was evident.

(3) The measurement of the gas phase velocity exhibited that, for the wavy interface region, the plane of maximum velocity shifted progressively towards the smooth upper wall as the gas flow rate was increased. The interfacial region had the similar structure as the turbulent flow over a rough surface.

(4) The eddy viscosity of the gas phase obtained in the vicinity of the wavy interface presented a much larger value than that estimated for the region close to a smooth solid wall in the single-phase turbulent flow.

(5) The analytical model for co-current stratified flow using the eddy viscosity hypothesis

which took into account the wave-induced shear stress, was presented and the numerical results agreed well with the experimental value.

But the mechanisms of these phenomena has yet to be sufficiently clarified. From the experimental point of view, the accumulation of detailed data is needed hereafter. And the problem of physical, not empirical, modelling of the effect of the interfacial waves still remains. The experimental work and the analytical study which takes into account the turbulent energy equations are now being undertaken.

REFERENCES

AGGOUR, M. A. & SIMS, G. E. 1978 A theoretical solution of pressure drop and holdup in two-phase stratified flow. *Proc. Heat Transfer and Fluid Mech. Inst.* 205–217.

AKAI, M., INOUE, A. & AOKI, S. 1977 Structure of a co-current stratified two-phase flow with wavy interface. *Theor. Appl. Mech.* **25**, 445–456.

ELLIS, S. R. & GAY, B. 1959 The parallel flow of two fluid streams: interfacial shear and fluid–fluid interaction. *Trans. Inst. Chem. Engrs* **37**, 206–213.

HANJALIĆ, K. & LAUNDER, B. E. 1972 Fully developed asymmetric flow in a plane channel. *J. Fluid. Mech.* **51**, 301–335.

HANRATTY, T. J. & ENGEN, J. M. 1957 Interaction between a turbulent air stream and a moving surface. *AIChE J.* **3**, 299–304.

HEWITT, G. F. & HALL-TAYLOR, N. S. 1970 *Annular Two-Phase Flow.* Pergamon Press, Oxford.

JOHANNESSEN, T. 1972 A theoretical solution of the Lockhart–Martinelli flow model for calculating two-phase flow pressure drop and hold-up. *Int. J. Heat Mass Transfer* **15**, 1443–1449.

LOCKHART, R. W. & MARTINELLI, R. C. 1949 Proposed correlation of data for isothermal two-phase, two-component flow in pipes. *Chem. Engng Prog.* **45**, 39–48.

MANDHANE, J. M., GREGORY, G. A. & AZIZ, K. 1974 A flow pattern map for gas–liquid flow in horizontal pipes. *Int. J. Multiphase Flow* **1**, 537–553.

MCELIGOT, D. M., SMITH, S. B. & BANKSTON, C. A. 1970 Quasi-developed turbulent pipe flow with heat transfer. *J. Heat Transfer, Trans. ASME* **92**, 641–650.

PATEL, V. C. & HEAD, M. R. 1969 Some observations on skin friction and velocity profiles in fully developed pipe and channel flows. *J. Fluid Mech.* **38**, 181–201.

THEOFANOUS, T. G., HOUZE, R. N., BRUMFIELD, L. K. & JOHNS, D. M. 1976 Structure of free boundary turbulence and interface mass transport. PCHE 76-1, Purdue University.